Hydrogen in aluminum: First-principles calculations of structure and thermodynamics

C. Wolverton
Ford Research and Advanced Engineering, MD3083/SRL, Dearborn, Michigan 48121-2053, USA

V. Ozoliņš
Department of Materials Science and Engineering, University of California, Los Angeles, California 90095-1595, USA

M. Asta
Department of Materials Science, Northwestern University, Evanston, Illinois 60208, USA

(Received 23 September 2003; revised manuscript received 23 December 2003; published 12 April 2004)

Despite decades of study, several key aspects of the Al-H system remain the subject of considerable debate. In an effort to elucidate some of these unknowns, we perform a systematic study of this system using first-principles density-functional calculations. We show that generalized gradient approximation (GGA) calculations provide an accurate picture of energetics, phase stability and structure, diffusion, and defect binding in the Al-H system. A series of calculations for hydrides in the *M*-H systems (*M*=Al, Ba, Ca, K, Mg, La, Li, Na, Ni, Pd, Sc, Sr, Ti, V, and Y) also shows that the GGA calculations are a quantitatively accurate predictor of hydride formation energies. For Al-H, we find: (i) In agreement with experiment, the observed metastable hydride, AlH_3 is found to have a small, negative formation enthalpy at ambient conditions, but a strongly positive formation free energy. (ii) Linear response calculations of AlH_3 yield vibrational frequencies, phonon densities of states (DOS), and heat capacities in excellent agreement with experimental measurements, and suggest the need for a reinterpretation of measured phonon DOS. (iii) Atomic relaxation and anharmonic vibrational effects both play an important role in the tetrahedral versus octahedral interstitial site preference of H in Al. (iv) The calculated heat of solution of H in the preferred tetrahedral site is large and positive (+0.71 eV), consistent with experimental solubility data and with Al as an endothermic hydrogen absorber. (v) Interstitial H interacts strongly with Al vacancies (□), with a calculated H-□ binding energy of 0.33 eV. (vi) In the absence of vacancies, the calculated migration energy of H between the tetrahedral and octahedral interstitial sites is 0.18 eV, but for H migrating away from an Al vacancy, the migration energy increases to 0.54 eV. Vacancy trapping of H can therefore provide an explanation for observed disparate H migration barriers.

DOI: 10.1103/PhysRevB.69.144109 PACS number(s): 81.30.Bx, 66.30.−h, 61.72.Bb, 61.72.Ji

I. INTRODUCTION

The subject of hydrogen in metals is a classic scientific problem as well as being technologically relevant due to the impact hydrogen can have on a material's properties.[1–6] The impact can be beneficial, as in the case of hydrogen storage, but hydrogen in materials is probably more famous as a deleterious addition, e.g., hydrogen embrittlement. Hydrogen also induces porosity and hence limits fatigue life in cast aluminum alloys due to the large solubility difference of H in liquid and solid aluminum.[7,8] Models of H-induced porosity in Al and its alloys[9,10] rely on quantities such as hydrogen solubility and diffusion which are still a subject of considerable debate, even in pure Al. Thus, in addition to being a model physical system for H in metals, understanding H in Al and Al alloys is of considerable importance for a variety of applications.

There is a wealth of experimental and previous theoretical work on H in Al (see, e.g., work cited in Refs. 7,8,11). However, even for many basic structural, energetic, and kinetic properties of this system, consensus is lacking and open questions still remain.

(1) *Site preference*: Hydrogen is well known as an interstitial impurity in many metals. Although the site preference for H in fcc metals is typically in octahedral (O_h) interstices, one experiment on the Al-H system suggests that the tetrahedral (T_d) site is preferred[12] whereas theoretical studies of H in Al have suggested preferred T_d,[13–15] O_h,[16–18] and even substitutional[19,20] sites.

(2) *Dilute heat of solution*: Measurements of the dilute heat of solution[21–25] are typically in the range +0.6 to +0.7 eV. However, calculations of this quantity range from +1.3 eV (Ref. 13) to −0.2 eV.[15]

(3) *Diffusion and H-vacancy binding*: The solubility of H in solid Al is extremely low (with atomic H/Al fractions in the range of 10^{-6} to 10^{-8}), thus hampering accurate diffusion measurements. The diffusion measurements therefore show a significant scatter, and although many measurements show an activation for diffusion between 0.4 and 0.6 eV (see Ref. 26 and references therein), a recent study[27] has proposed that the activation is much lower (0.17 eV), with the discrepancy being due to binding or trapping sites for H. To explain various aspects of diffusion measurements, a significant H-vacancy binding has been suggested by some[13,27–31] but dismissed by others.[26]

We thus assert the need for a reexamination of the conflicting theoretical and experimental claims concerning the structure and phase stability of H in Al within a comprehensive, state-of-the-art, first-principles analysis. Given the contradictory nature of previous calculations, it is clear that any analysis of this type must include a critical assessment of the accuracy of the computational methods employed. In this

TABLE I. Convergence tests of VASP-GGA static (no vibrations) calculations on H in Al. All energies are in eV: $\delta E(T_d - O_h)$ is the energy difference between hydrogen in tetrahedral and octahedral interstices. [$\delta E(T_d - O_h) < 0$ indicates that tetrahedral sites are favored.] ΔE_{imp} is the $T=0$ energy of the hydrogen impurity in Al, relative to bulk Al and a H_2 molecule. Only GGA results are shown here, though LDA exihibited similar convergence properties.

Convergence test	Cell size	E_{cut} (eV)	**k** points	$\delta E(T_d - O_h)$	ΔE_{imp}
k points	32	237	$8\times8\times8$	-0.14	$+0.56$
	32	237	$16\times16\times16$	-0.13	$+0.69$
	32	237	$24\times24\times24$	-0.12	$+0.69$
Energy cutoff	32	237	$16\times16\times16$	-0.13	$+0.69$
	32	350	$16\times16\times16$	-0.13	$+0.69$
Cell size	32	237	$16\times16\times16$	-0.13	$+0.69$
	64	237	$8\times8\times8$	-0.13	$+0.70$
	108	237	$8\times8\times8$	-0.15	$+0.71$

paper, we investigate issues related to site preference, heat of solution, diffusivity, and vacancy binding of H in Al. In order to test the applicability of these calculations to the Al-H system, we have also considered the phase stability of the reported metastable AlH_3 hydride, as well as Al-H in several commonly occuring (but unreported in the Al-H system) hydride structures. Also, as a more general test of first-principles methods to metal-hydrogen phase stability, we have performed a series of calculations for metal hydride formation energies, and compared our results with experimental values. Our calculations are based on density-functional theory, both in the local-density (LDA) and generalized gradient approximations (GGA). We demonstrate that GGA calculations provide an accurate and consistent picture of the structure and energetics of the Al-H system.

II. METHODOLOGY

Our electronic-structure calculations are based on density-functional theory (DFT),[32,33] with core-electron interactions described by ultrasoft pseudopotentials,[34,35] as implemented in the highly efficient VASP code.[36–39] For exchange correlation, we use both the LDA with the exchange-correlation functional of Ceperley and Alder,[40,41] as well as the GGA of Perdew and Wang.[42] We solve the Kohn-Sham equations iteratively, and unless otherwise mentioned, we optimize all atomic positions, cell shape, and cell volume using either a conjugate gradient or Newton-Raphson algorithm. We expand the one-electron wave functions in a plane-wave basis with an energy cutoff as large as 350 eV, although convergence tests (described below) indicate that 237 eV (= 17.5 Ry) is a sufficient cutoff to achieve highly accurate energy differences. Extensive tests of **k**-point sampling using Monkhorst-Pack[43] *k*-point meshes (using from $8\times8\times8$ to $24\times24\times24$ grids) indicate that total energies for all cells are converged to within ~ 0.01 eV. We employ a Fermi smearing of the electronic occupancy with a fictitious electronic temperature of 0.05 eV. For the ordered hydride structures, we use primitive unit cells (2–24 atoms), whereas for the description of H impurities, we construct supercells containing 32, 64, and 108 Al-atom sites.

Table I gives convergence properties of the impurity calculations with respect to energy cutoff, **k**-point sampling, as well as supercell size. We find that a relatively modest energy cutoff (237 eV) and supercell size (32 Al atoms) produce converged energetic results, provided that an extremely dense **k**-point mesh ($16\times16\times16$) is used. Our finding of the necessity of using a dense **k**-point mesh in computing defect properties in Al is consistent with similar conclusions from previous work.[44,45]

For the migration energy calculations, we exploit the very high symmetry of the problem. We simply place the hydrogen between the T_d and O_h positions at the distance of closest approach to Al, and subsequently relax all atomic positions (but not cell vectors) with a Newton-Raphson algorithm. Using this approach, the system always converges to a geometry with an energy higher than either the T_d or O_h positions, with the converged position of the hydrogen nearly midway between the high-symmetry positions.

Zero-point effects were included in many of the results presented here. Vibrational properties of H interstitials were obtained using two distinct methods: (i) calculation of a full dynamical matrix using the frozen phonon approach, and (ii) a more simplistic Einstein model for localized H modes. Using the frozen phonon approach,[46] we study the $\mathbf{q}=0$ phonon states of 32-atom supercells. For each cell, all symmetry inequivalent rows of the $\mathbf{q}=0$ dynamical matrix were determined, with the remaining rows given via standard symmetry-group transformations.[47] Individual elements $D^{ij}_{\alpha\beta}$ of the $\mathbf{q}=0$ dynamical matrix are proportional to the force acting on the atom i along the Cartesian direction α if the atom j is displaced by a small amount along the direction β, $F^i_\alpha = -\sqrt{M_i M_j} D^{ij}_{\alpha\beta} u^i_\beta$. For each symmetry-inequivalent choice of u^i_β, the forces F^i_α were obtained for a set of nine evenly distributed displacements around the equilibrium position, from $u^i_\beta = -0.04$ Å to $u^i_\beta = +0.04$ Å. The calculated Hellman-Feynman forces were fit using third-order splines, and the linear terms were used to extract $D^{ij}_{\alpha\beta}$.

In the Einstein model, vibrational frequencies are determined from the energy-versus-displacement curves of H atoms alone. The total energies are calculated using the full 32-atom supercell, and thus include contributions from all atoms. An approximation is made for phonon eigenvectors

where one assumes that Al atoms are essentially static and cannot participate in vibrations at the frequencies of local H modes. Due to the large disparity in atomic masses of H and Al and clear separation of high-frequency H modes from Al phonons, this is usually a very good approximation. The movement of Al atoms can be taken into account approximately by substituting the H atomic mass with an effective reduced mass $1/\mu=(1/m_H)+(1/nm_{Al})$, where n is the number of Al atoms participating in the mode. For vibrations in the O_h site, for instance, one could assume that H vibrations are essentially those of H in a linear triplet of atoms Al-H-Al, in which case n is approximately 2, resulting in $\mu \sim 0.98 m_H$. Thus, using μ instead of m_H produces only a 1% correction to the frequency; due to uncertainties involved in determining the appropriate value of n, we have neglected this small correction and used $\mu=m_H$ everywhere. Comparison of the frozen-phonon and Einstein models allows one to determine the accuracy of the latter approach, which is found to be very good, as discussed below in Sec. IV B.

In a few cases (particularly for octahedral interstitial positions), the calculated potential-energy wells were quite flat, and the corresponding vibrational frequencies were quite low. These observations raise the possibility of important anharmonic contributions to the vibrational energies. Anharmonic effects were investigated within the Einstein model by considering larger displacements along the $\langle 100\rangle$, $\langle 110\rangle$, and $\langle 111\rangle$ directions, and fitting the potential energy to a functional form of T_d or O_h symmetry

$$V(x,y,z)=\frac{k}{2}(x^2+y^2+z^2)+a(x^4+y^4+z^4) + b(x^2y^2+y^2z^2+x^2z^2)+\delta xyz, \qquad (1)$$

where $\delta=0(\neq 0)$ for the O_h (T_d) site symmetry. The coefficients k, a, b, and δ were fit to the calculated energetics out to 0.4 Å displacements. The three-dimensional(3D) Schrödinger equation was then solved numerically for the potential of Eq. (1) using an expansion in the eigenfunction basis of the harmonic oscillator. A perturbative approach was also attempted, but in several cases, the anharmonic zero-point effects were found to be quite large and the potentials were so strongly anharmonic that perturbation theory on the harmonic oscillator results was not meaningful (a full numerical solution was required).

Finally, vibrational properties of ordered compounds were determined using the density-functional linear-response method. Details of this approach have been described in previous publications.[48] Here we only mention that a Troullier-Martins-type H pseudopotential was generated using a cutoff radius $r_{cs}=0.4$ bohr.

For each of the above computational approaches, a variety of vibrational properties (e.g., vibrational entropy, root-mean-square displacement of atoms, etc.) can be extracted from calculated phonon wave functions, frequencies, and modes, using standard expressions.[47]

TABLE II. Comparison of first-principles calculated (LDA and GGA) and experimental structural properties of AlH_3 as well as some fluorite and rocksalt hydrides. Lattice constants (a,c) are in Å, and x_H is the cell-internal position for H (space group $R\bar{3}c$). ΔE is the formation energy [Eq. (2)] of the AlH_3 hydride in eV/atom. Unless otherwise indicated, calculated results are from the present work. Note that zero-point effects are not included in the calculated results in this table. All calculated results from the present work in this table are calculated using $E_{cut}=350$ eV.

Hydride	Property	LDA	GGA	Expt.
AlH_3	a	4.25	4.42	4.449 [a]
	c	11.66	11.80	11.804 [a]
	c/a	2.74	2.67	2.653 [a]
	x_H	0.663	0.634	0.628 [a]
	ΔE	−0.134	−0.039	−0.030 [b]
ScH_2	a	4.69 [c]	4.80	4.78 [d]
TiH_2	a	4.34 [c]	4.43	4.44 [d]
VH_2	a	4.13 [c]	4.22, 4.22 [e]	4.27 [d]
NiH	a	3.64 [c]	3.73	3.72 [d]

[a]Reference 49.
[b]Reference 53—formation enthalpy at ambient conditions.
[c]Reference 51.
[d]Reference 6.
[e]Reference 52.

III. RESULTS: METAL HYDRIDES

A. Al hydride, AlH_3: $T=0$ static energetics

Although aluminum has no stable hydrides (at low pressures), there have been several reported metastable hydrides. Turley *et al.*[49] reported five crystalline forms of nonsolvated aluminum hydride, and found the crystal structure of the one which they classify as ''most stable,'' AlH_3. This compound is trigonal (space group $R\bar{3}c$) with eight atoms per primitive unit cell. A comparison of the first-principles calculated and experimental structural parameters of AlH_3 is given in Table II. Typically, LDA calculations of crystalline compounds underestimate lattice parameters with respect to experiment by $\sim 1-2\%$ whereas GGA calculations may overestimate a similar amount. However, this compound is not typical in the sense that it is a hydrogen-rich solid, and therefore the typical errors of DFT calculations may not hold. We see from Table II that the LDA lattice parameters of AlH_3 are underestimated by a few percent, as is typical. The GGA calculations are significantly closer to experiment, but still slightly underestimate the lattice parameters. The level of agreement between the calculated and experimental results indicates that first-principles methods seem to be reasonably accurate for the Al-H system, and that GGA may be more accurate than LDA for this system.

In order to test the generality of these conclusions, we also compare in Table II the LDA/GGA calculated static[50] lattice constants of several fluorite- and rocksalt-based hydrides with experiment. We include both present results (see below) and also some recent calculations of hydrides using both LDA (Ref. 51) and GGA.[52] The comparison for ScH_2, TiH_2, VH_2, and NiH indicate the same trends that were

found for AlH_3. LDA underestimates the lattice parameters (sometimes significantly), GGA is closer to experiment, either slightly underestimating or overestimating the lattice parameter. (We note that although the energetic properties in Table I were converged with an energy cutoff of 237 eV, converged structural properties require a larger cutoff, and hence, all of the results in Table II were calculated using a cutoff of 350 eV; all other results in the present work are calculated using $E_{\mathrm{cut}}=237$ eV.)

In addition to the structural properties of AlH_3, we have also investigated the phase stability of this and other (hypothetical) Al-H compounds. We have computed the energetics of Al-H in several commonly occuring hydride structures: AlH (rocksalt and zincblende), AlH_2 (fluorite and rutile), and AlH_3 (AlH_3 and YH_3). The calculated formation energies are shown in Fig. 1. All of the hydrides are quite unstable with respect to decomposition ($\Delta E>0$) except for the observed AlH_3 phase, which has a small, but negative ΔE. ΔE is the energy of the Al_pH_q hydride relative to pure Al and an isolated H_2 molecule:

$$\Delta E(\mathrm{Al}_p\mathrm{H}_q)=\frac{1}{p+q}\left[E(\mathrm{Al}_p\mathrm{H}_q)-pE^{\mathrm{fcc}}(\mathrm{Al})-\frac{q}{2}E(\mathrm{H}_2)\right]. \tag{2}$$

(Analogous expressions exist for other quantities, e.g., the formation entropy ΔS, or formation free energy ΔG.) Although both LDA and GGA show the observed AlH_3 compound as lower in energy than any of these other competing structures, the quantitative energies differ: GGA gives $\Delta E=-0.039$ eV/atom, while LDA gives $\Delta E=-0.134$ eV/atom.

The energetics of LDA vs GGA in Fig. 1 for Al-H look similar, except for a composition-dependent "shift." In Fig. 1(c), we illustrate this observation by shifting the LDA energy of the H_2 molecule in Eq. (2) by 0.25 eV/H_2. We call these shifted-LDA results LDA*. The value of the energy shift is chosen so as to bring the LDA* value of $\Delta E(AlH_3)$ into agreement with GGA. This simple shift of the LDA results brings all of the LDA* energies into much better agreement with the GGA results. This comparison indicates that the majority of the difference in ΔE between LDA and GGA results from the description of the H_2 molecule. Below, we quantitatively compare the values of ΔE of AlH_3 with experimental calorimetry results and confirm the accuracy of the GGA results.

Another way to see the extent to which the description of the H_2 molecule is responsible for the LDA/GGA differences is to consider energy differences for which the energy of H_2 does not appear. For instance, the energetic difference between the two structures at AlH_3 same composition is independent of the calculated energy of H_2: $\delta E(AlH_3-YH_3\text{-type})=-0.11$ (LDA) and -0.14 (GGA) eV/atom. These numbers are much more similar than the LDA/GGA difference between $\Delta E(AlH_3)$.

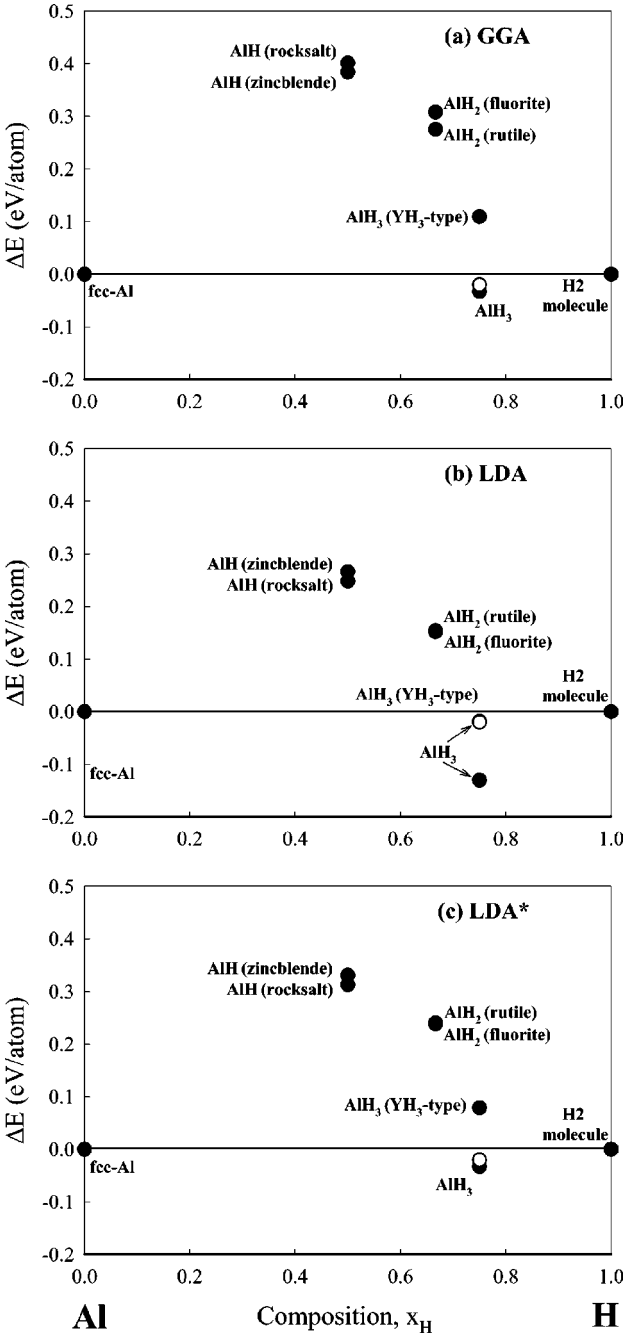

FIG. 1. First-principles calculated formation energies ΔE [Eq. (2)] of ordered Al-H hydrides using (a) GGA, (b) LDA, and (c) a modified LDA in which a constant is added to the energy of the H_2 molecule to make the formation energy of the AlH_3 phase equal to the GGA-calculated value. Open circles represent the experimental results of Ref. 53. From the similarity of results in (a) and (c) one can see that a large portion of the difference between LDA and GGA for the Al-H system lies simply in the energy of the reference molecule, H_2. Note that zero-point effects are not included in the energetics of this figure.

B. Al hydride, AlH_3: Vibrations and thermodynamics

Vibrational properties of AlH_3 were obtained using the DFT linear-response formalism within the LDA. The calculated phonon density of states (DOS) is given in Fig. 2. We find that the phonon modes of AlH_3 are grouped in three frequency regions: (i) low-frequency vibrations of Al atoms below 50 meV (three acoustic and three optical branches),

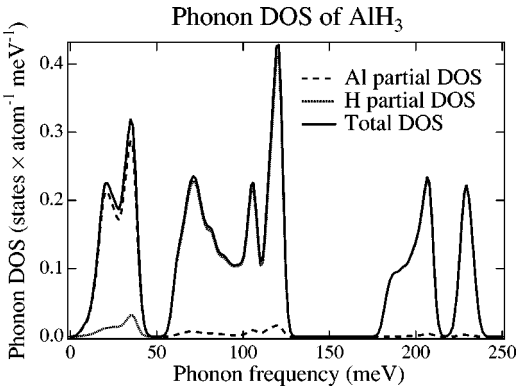

FIG. 2. Calculated phonon density of states (DOS) in trigonal AlH_3, obtained using the LDA and experimental structural parameters. Phonon frequencies were calculated on a regular $8\times8\times8$ mesh of wave vectors and their contributions to the total DOS were represented by Gaussians of width 25 cm^{-1}.

(ii) rotational motions and H-Al-H bond-bending deformations of corner-sharing AlH_6 octahedra between 50 and 125 meV (12 modes), and (iii) Al-H bond-stretching motions of H above 175 meV (six modes). Comparison with inelastic neutron scattering (INS) data obtained from AlH_3 powders[54] shows a good agreement for the positions of the main peaks for the first two groups of phonon modes (up to 125 meV). The experimental data of Ref. 54 was analyzed using a frequency cutoff below 140 meV; peak structure in the INS spectra at higher energies was attributed to two-phonon and higher scattering processes. Our results cast doubt on this analysis, since we find additional phonon states above 175 meV, corresponding to Al-H stretch modes. Closer examination of the raw INS data in Ref. 54 clearly shows additional two-peak structure at 200 and 240 meV, which matches very well with our calculated positions of high-frequency peaks in Fig. 2. Reinterpretation of the experimental INS data using a more accurate model of lattice dynamics would be very interesting. Calculated frequencies of zone-center modes, which can be accessed by infrared and Raman scattering techniques, are given in Table III, together with the calculated high and low-frequency dielectric constants. These values have not yet been measured experimentally.

The vibrational enthalpy and free energy were evaluated from the directly calculated phonon frequencies using a regular $8\times8\times8$ grid of wave vectors. The calculated value of the $T=0$ K vibrational enthalpy is $H^0_{\rm vib}(AlH_3)=+161$ meV/atom. Using the calculated LDA linear-response values of $H^0_{\rm vib}({\rm Al})=+40$ meV/atom and $H^0_{\rm vib}(H_2)=+130$ meV/atom, we find that zero-point vibrations destabilize the AlH_3 compound by $\Delta H^0_{\rm vib}(AlH_3)=+53$ meV/atom. We note that the size of this energetic effect is rather large, overwhelming the GGA-calculated formation energy.[55] At $T=300$ K the vibrational enthalpy is essentially unchanged: $\Delta H^{T=300\ {\rm K}}_{\rm vib}(AlH_3)=+56$ meV/atom.[56] Subtracting the enthalpy of H_2 gas, $\frac{7}{2}k_BT$ per H_2 molecule,[57] we obtain that at $T=300$ K dynamical (vibrational and kinetic energy) contributions to the formation enthalpy of AlH_3 give $\Delta H^{T=300\ {\rm K}}_{\rm dyn}(AlH_3)=+21$ meV/atom. Adding these dynamical contributions to the static energies above yields $\Delta H^{T=300\ {\rm K}}_{\rm LDA}=-113$ meV/atom and $\Delta H^{T=300\ {\rm K}}_{\rm GGA}=-18$ meV/atom. We note in the latter case, the (LDA calculated) positive dynamical contributions largely cancel the slightly negative static formation energy predicted by the GGA.

TABLE III. LDA linear-response calculations of the zone-center phonon frequencies (in cm^{-1}) in bulk AlH_3 at the experimental structural parameters. Only infrared-active modes have distinct longitudinal optical (LO) and transverse optical (TO) frequencies. The independent components of high- and low-frequency dielectric tensors are calculated to be $\epsilon^\infty_\parallel=5.0$, $\epsilon^\infty_\perp=4.8$, $\epsilon^0_\parallel=14.3$, and $\epsilon^0_\perp=10.0$ for directions parallel and perpendicular to the trigonal axis, respectively. Electronic bonding is predicted to be highly ionic, as indicated by the eigenvalues of Born effective charges: $Z^\parallel_{\rm eff}({\rm Al})=+2.81$, $Z^\perp_{\rm eff}({\rm Al})=+2.61\pm0.55i$, $Z^\parallel_{\rm eff}({\rm H})=-1.43$, $Z^\perp_{\rm eff}({\rm H})=-0.62$, where "$\parallel$" and "$\perp$" refer to the trigonal axis.

Symmetry	$\nu_{\rm TO}$	$\nu_{\rm LO}$
IR-active modes		
E_u	286	293
A_{2u}	512	777
E_u	583	635
E_u	851	1008
A_{2u}	1650	1833
E_u	1687	1836
Raman-active modes		
E_g	490	
A_{1g}	812	
E_g	993	
E_g	1481	
Silent modes		
A_{1u}	345	
A_{2g}	751	
A_{1u}	921	
A_{2g}	1903	

We next turn to a quantitative comparison of ΔH with experimental calorimetric results. Sinke *et al.*[53] performed calorimetric measurement of the heat of formation of AlH_3. At room temperature, the AlH_3 phase is thermodynamically unstable with respect to decomposition into Al and H_2,[53] however, these authors found a very small but negative formation enthalpy, $\Delta H=-0.030\pm0.002$ eV/atom. One should note that this formation enthalpy is extremely small, and thus the agreement between these values from calorimetry and our GGA calculated value of $\Delta H^{T=300\ {\rm K}}_{\rm GGA}=-0.018$ eV/atom is quite reasonable (it is well within the expected accuracy for these types of calculations). Thus, the formation enthalpy of AlH_3 gives another indication that GGA provides a more accurate description of Al-H than does the LDA.

Sinke *et al.*[53] also determined the heat capacity of AlH_3, C_v. For an insulator at ambient conditions, C_v is given by the harmonic vibrational contribution, which can be easily evaluated from the calculated phonon DOS of AlH_3. The result of this calculation is shown in Fig. 3, demonstrating that the average phonon frequencies, and thus their contribu-

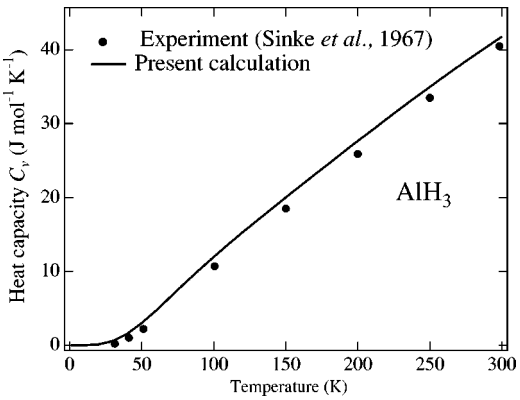

FIG. 3. Comparison of the calculated (solid line, evaluated using the phonon DOS in Fig. 2) and measured (symbols, calorimetry data from Ref. 53) heat capacities C_v of AlH_3.

tions to thermodynamic functions, are given accurately by the LDA linear-response method.

To this point, we have only considered the energies and enthalpies of aluminum hydrides. Of course, the actual observed metastability of AlH_3 is governed by free energy, including entropic effects. In particular, the free energy of the H_2 molecule is dramatically effected by entropic effects at finite temperatures. To get the more realistic free energy of H_2, the first-principles value of the $T=0$ H_2 molecule can be supplemented with the standard enthalpy and entropy of H_2 gas (e.g., see Ref. 58)

$$G(\mathrm{H_2}) = E^{\text{first-principles}}(\mathrm{H_2}) + \tfrac{7}{2}k_B T - TS^{\text{expt}}(\mathrm{H_2}), \qquad (3)$$

where $S^{\text{expt}}(\mathrm{H_2}) = 130.684$ J/K mole of H_2 at STP ($\sim 15.7\ k_B/\mathrm{H_2}$). [Combining GGA-calculated $T=0$ molecular energies with standard entropies has been used previously to successfully describe the energetics of the dehydration of $HAlO_2$ into γ-Al_2O_3.[59]] In addition to the entropic contributions due to the H_2 gas, there are also vibrational entropy contributions due to the solid-state phases. The first-principles calculated vibrational entropy of formation of AlH_3 at $T=300$ K is

$$\Delta S^{300}_{\text{vib}}(\mathrm{AlH_3}) = \tfrac{1}{4}[S^{300}_{\text{vib}}(\mathrm{AlH_3}) - S^{300}_{\text{vib}}(\mathrm{Al}) + \tfrac{3}{2}S^{300}_{\text{vib}}(\mathrm{H_2})]$$
$$= 0.2\ \ k_B/\text{atom}.$$

This is a small contribution in comparison with the entropy of the gas of H_2 molecules. Using this vibrational contribution along with Eq. (3) as the energetic reference of H_2 (with the very small vibrational entropy contribution of H_2 removed, so as to avoid double counting this term), our GGA calculated value of $\Delta H^{T=300\ \mathrm{K}}_{\mathrm{GGA}} = -0.018$ eV/atom at room temperature becomes $\Delta G^{T=300\ \mathrm{K}}_{\mathrm{GGA}} = +0.129$ eV/atom, indicating that the AlH_3 phase, while possessing a slightly negative ΔH, is unstable with respect to decomposition at room temperature. This positive formation free energy is in excellent agreement with both the observed metastability of the compound, and with the free energy of formation at room temperature and pressure measured by Sinke *et al.*, $\Delta G(T = 300\ \mathrm{K}) = +0.120 \pm 0.025$ eV/atom. We summarize all of the calculated thermodynamics of AlH_3 in Fig. 4.

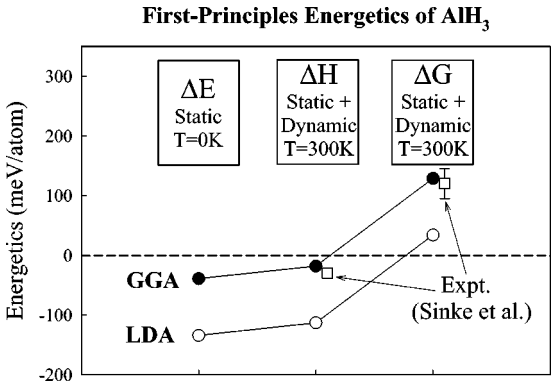

FIG. 4. First-principles calculated thermodynamics, ΔE, ΔH, and ΔG of AlH_3. The calculated results of ΔE are given by LDA and GGA first-principles total energies of the static $T=0$ K formation energy. ΔH at ambient conditions is given by a combination of the values of ΔE, supplemented by dynamic contributions: vibrational energies from (LDA) linear-response calculations, and kinetic energy considerations of the H_2 gas. The values of ΔG (ambient conditions) are obtained by adding the entropic contributions to ΔH, vibrational entropies are calculated via first-principles (LDA) linear-response calculations, and the entropy of H_2 is given from standard equations of state for the gas phase. Also shown are the experimental results of Sinke *et al.* (Ref. 53), demonstrating the high accuracy of the GGA calculated thermodynamics.

Lattice expansion due to anharmonic zero-point effects also appears to be sizable. We have calculated the changes in the LDA phonon frequencies upon (i) an isotropic expansion of linear lattice dimensions by 1.2%, (ii) volume-conserving change in the c/a ratio by 1.5%, and (iii) 1.7% change in the reduced coordinate (x) of H atoms. The resulting changes in the vibrational free energies were expressed as linear forms of these three independent structural parameters. As expected, volume change had the largest relative effect on phonon frequencies, followed by the change in H coordinate, while change in the c/a ratio had hardly any effect on the calculated free energies. The static lattice energy was calculated at a series of small finite differences around the LDA equilibrium value and fitted by a quadratic form involving three independent variables and six unknown coefficients. The total free energy was minimized as a function of temperature, yielding the equilibrium structural parameters including quasiharmonic vibrational effects. We found that the lattice parameter changes by $\delta a(T=0\ \mathrm{K})/a = 1.3\%$ and $\delta a(T=300\ \mathrm{K})/a = 1.4\%$ at $T=0$ and 300 K, respectively. Almost all of the increase in the lattice parameter is due to large zero-point energy effects, raising an interesting possibility that lattice parameters of metal hydrides may be substantially affected by zero-point effects. We note that adding these (LDA calculated) lattice expansion effects to the GGA calculated structural properties of AlH_3 (Table II) yields lattice parameters that are slightly larger than experiment, not uncommon in GGA calculations.

C. Structure and stability of other metal hydrides

In the condensed-matter physics community, previous studies using DFT-based methods have shown that formation

TABLE IV. Comparison of present first-principles (VASP-GGA) energies and measured enthalpies of formation for several metal hydrides MH_q. The energy of formation is defined as $\Delta E(MH_q)=E(MH_q)-[E(M)+(q/2)E(H_2)]$. All energies given in kJ/0.5 mol H_2. (1 kJ/mole≡10.36 meV.) All experimental values are enthalpies and are referenced and discussed in more detail in Ref. 5, except where indicated. Note that zero-point effects are not included in the calculated results in this table. [All calculated results were performed using a cutoff energy of 237 eV, and are fully relaxed with respect to all cell-external and cell-internal degrees of freedom. As a test of convergence of these energies, a few hydride formation energies are also shown, in parentheses, with a larger cutoff of 350 eV, yielding only small differences ($\lesssim$1 kJ/0.5 mol H_2) with the lower cutoff calculations.]

Compound	Structure	GGA (ΔE)	Expt. (ΔH)
AlH_3	AlH_3	−4.2 (−5.0)	−3.9 [a], −15.3 [b]
BaH_2	$CoSi_2$	−71	−88.5 [b]
CaH_2	$CoSi_2$	−86	−91.8 [b], −92.0 [c],−85.1 [c]
KH	NaCl	−41	−57.7 [b], −57.3, −59.1, −63.4, −57.8
MgH_2	TiO_2	−32	−37.6 [b], −33.5, −37.2, −32.9
LaH_2 [f]	CaF_2	−95	−95.6
LaH_3 [f]	BiF_3	−78	
LiH	NaCl	−87	−90.5 [b], −90.4, −89.3, −90.6
NaH	NaCl	−43	−56.3 [b], −56.9, −56.4
$NaAlH_4$ [g]	$NaAlH_4$	−16	−18.5 [d]
Na_3AlH_6 [g]	α-Na_3AlH_6	−25	−23.5 [d]
NaH	NaCl	−43	−56.3 [b], −56.9, −56.4
NiH_x	NaCl	−7.5 (−7.5)	−5.0, −4.4, −8.2, −4.5
PdH_x	NaCl/A_2B_2	−18	−19.2
ScH_2	CaF_2	−100 (−100)	−129, −100.5
SrH_2	Co_2Si	−84	−90.2 [b], −99.6 [c]
TiH_2	CaF_2	−76 (−75)	−62.6, −72.2, −66.5, −65.2
V_2H	β_1-V_2H	−42	−40.6
VH_2	CaF_2	−33 (−32)	−19.1
YH_3	YH_3	−79	−79.8 [e]
YH_2	CaF_2	−105	−105.0 [e]

[a]Reference 53.
[b]Reference 62.
[c]Reference 6.
[d]Reference 63.
[e]Extrapolated to zero temperature.
[f]PAW (GGA) potentials used for La-H calculations.
[g]For sodium alanates, the reactions considered are $3NaAlH_4 \rightarrow Na_3AlH_6 + 2Al + 3H_2$ and $Na_3AlH_6 \rightarrow 3NaH + Al + \frac{3}{2}H_2$.

energies between *solid-state constituents* are often quantitatively accurate. For instance, see Fig. 1 of Ref. 60 for a comparison between DFT and experimental formation energies for a series of Al-based intermetallic compounds, showing a typical agreement to within 1 or 2 kJ/mol of atoms. However, it is well known in the chemistry literature (see, e.g., Ref. 61) that DFT methods typically do not provide quantitatively reliable heats of formation for reactions between *atomic and molecular constituents*. In the present work, we have a situation somewhat intermediate in that we are concerned in Eq. (2) with a reaction between one solid and one molecular constituent, producing a solid hydride.

Hence, one would like to understand whether the good agreement between first-principles and calorimetric values of formation energies/enthalpies for the AlH_3 compound is accidental, or an indication of a more general validity of first-principles methods for hydride systems. To that end, we have computed the static, $T=0$ formation energies of several other metal hydrides. In addition to AlH_3, we have computed values of ΔE [Eq. (2)] for hydrides in the M-H systems, M = Al, Ba, Ca, K, Mg, La, Li, Na, Ni, Pd, Sc, Sr, Ti, V, and Y, as well as the sodium alanates, $NaAlH_4$ and Na_3AlH_6. The crystal structures of these hydrides encompass ten distinct crystal structures: rutile, rocksalt, fluorite, YH_3-type, AlH_3-type, Co_2Si-type, β_1-V_2H, BiF_3-type, $NaAlH_4$, and α-Na_3AlH_6. (Additionally for the Pd-H system, we have considered a $PdH_{0.5}$ rocksalt-based A_2B_2 ordered vacancy compound, which has been observed in low-temperature neutron diffraction experiments—see discussion and references in Ref. 5.) These first-principles calculated energies are compared with measured values of ΔH in Table IV and Fig. 5. The first-principles formation energies are almost all within 10–15 kJ/mol of H (0.1–0.15 eV/H atom) of the experimentally determined enthalpies. (Whenever possible, ex-

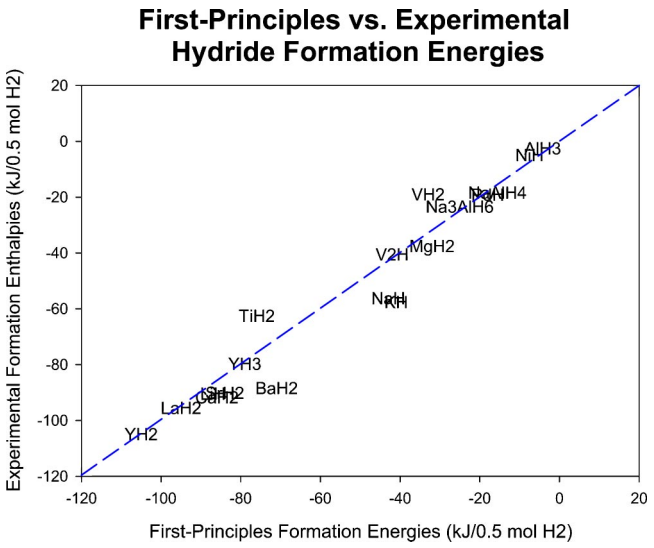

FIG. 5. Comparison of present first-principles (VASP-GGA) energies and measured enthalpies of formation for several metal hydrides MH_q. The energy of formation is defined as $\Delta E(MH_q) = E(MH_q) - [E(M) + (q/2)E(H_2)]$. All energies given in kJ/0.5 mol H_2. (1 kJ/mole≡10.36 meV.) For each hydride, experimental enthalpy values in Table IV are averaged. Note that zero-point effects are not included in the energetics of this figure.

perimental numbers were taken from low or room-temperature experiments so as to minimize the distinction between theory and experiment due to the PV and C_V terms in the enthalpy. However, some of these experimental numbers are from as high as 1000 °C which is approximately $k_B T \sim 10$ kJ/mol.) Given that zero-point and finite temperature effects are not considered in the calculated results, the agreement between first-principles calculated and experimental hydride energetics seems quite good across a wide variety of structural types and local hydrogen coordinations. This comparison gives us confidence in the applicability of our methods to these hydrogen/metal systems.

Although many previous reports of first-principles studies of metal hydrides exist, only a few report formation energies. Consistent with the present work, these previous papers have also generally found good agreement between first-principles and experiment for alkali hydrides,[64] NbH,[65] Mg_2NiH_4,[66] TiH_2 and VH_2,[52] $LaNi_5H_7$,[67] sodium alanates,[68] as well as a series of group I, II, and transition-metal hydrides.[51] Miwa and Fukumoto[52] used GGA, but found $a \sim 10$ kJ/0.5 mol H_2 underestimate of the formation energies of TiH_2 and VH_2 with respect to experiment. These results are consistent with our calculated results for TiH_2 and VH_2. However, these authors also calculated zero-point energies of the hydrides of the order of 10 kJ and assert that the bulk of the discrepancy between experiment and GGA can be accounted for with zero-point effects. Recently, Smithson *et al.*[51] have used VASP within the LDA to study as series of metal hydride energetics. Many of the hydride energies in this paper seem to be ~ 0.25 eV/H_2 lower than experiment. Interestingly, it appears as though these results are shifted with respect to experiment by a very similar amount to the ''LDA shift'' made in H_2 that we deduced in the preceding section to reconcile LDA and GGA energies of AlH_3.

IV. RESULTS: HYDROGEN IN ALUMINUM

Now that we have gained some confidence in the applicability of our first-principles methods to metal-hydrogen systems, we return to the subject of H in Al. We have applied our first-principles methods to studying the site preference, vibrational states, dilute heat of solution, vacancy binding, and diffusion of H in Al.

A. Site preference

The site preference of H has been the subject of many previous investigations. Bugeat *et al.*[12] implanted hydrogen and deuterium in Al, and used channeling and nuclear analysis experiments at 33 K to deduce an interstitial T_d site preference. Aside from this one experimental determination, most of the indication of site preference have come from computational studies. Unfortunately, these studies have not helped to clarify the situation. H in Al was a benchmark system for early studies for calculations of the electron density (both non-self-consistent and self-consistent) employing approximate schemes for treating the metal lattice. These approaches include treating the metal lattice as jellium, in a perturbative manner, or by a spherical average of host-ion potentials. Some of these approaches found a preferred O_h occupancy,[17,18] although others found T_d site preference,[13,14] and some have even indicated a preference for the substitutional position.[19,20] Using an effective medium theory approach, Puska and Niemenen[69] found an O_h site preference. More recent work includes an embedded atom method study[16] (showing an O_h preference) as well as first-principles DFT-based studies.[15,70] Reference 15 uses the LDA and indicates a T_d preference of H, but does not consider the effect of zero-point energies on the site preference. In sum, the theoretical studies of site occupancy of H in Al are controversial, and the only available experimental report seems to indicate a T_d preference.

For our T_d and O_h impurity calculations, both the cell-internal and cell-external degrees of freedom are relaxed. The energetics of H in interstitial T_d vs O_h sites are given in Table I. $\delta E(T_d - O_h)$ is the energy difference between hydrogen in tetrahedral and octahedral interstices. $\delta E(T_d - O_h) < 0$ indicates a tetrahedral site preference. Tetrahedral sites are clearly favored qualitatively in all calculations (both LDA and GGA) based on static, $T=0$ energetics only. We consider vibrational effects on the site preference below.

The fact that the T_d vs O_h energy difference is quite small is consistent with reports of size-based site preferences of hydrogen in metals. In a study of transition-metal hydrides, Irodova *et al.* (see Ref. 71 and references therein) found a correlation between the type of interstices occupied by hydrogen atoms and the size of the metal atoms. For large metal atoms, T_d sites are preferred, with O_h sites preferred for small metal atoms. The change in the coordination occurs at some critical atomic radius of the metal $\sim r = 1.34$–1.40 Å (with the range depending on the row of the

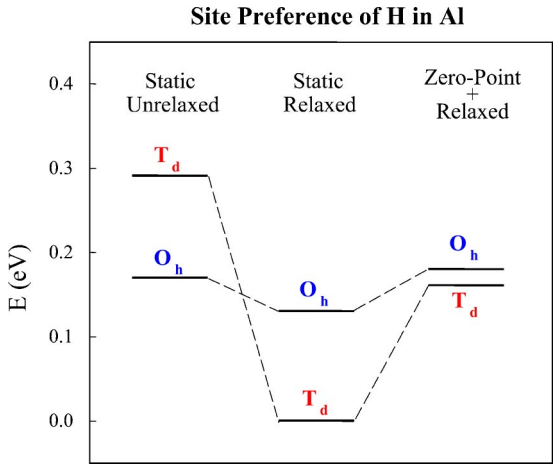

FIG. 6. Physical contributions to the T_d/O_h site preference of H in Al. Note that in static, unrelaxed calculations, H energetically prefers the larger O_h site. However, atomic relaxation is larger in the T_d site, qualitatively reversing the static site preference. Vibrational frequencies of H in the T_d site are larger than in the O_h site, thus giving a larger zero-point energy in the T_d site. When all contributions are considered, the calculations predict a small preference for H in T_d sites at $T=0$, consistent with the experimental report of Bugeat *et al.* (Ref. 12).

transition metal host). The nearest-neighbor distance of fcc Al is 2.86 Å, leading to $r_{\mathrm{Al}}=1.43$ Å. It is interesting that our results are consistent with this idea of a size-mediated site preference (although it should be remembered that the study of Irodova *et al.* is for hydrogen in transition-metal alloys) The atomic radius of Al is larger than, but close to the critical radius predicted by Irodova, thus indicating a slight preference for T_d sites over O_h.

Motivated by this indication of a size-mediated site preference, we have examined the physical contributions of static atomic relaxation and H vibrational frequencies on the site preference (Fig. 6).

Static atomic relaxation. In Table V, we also show results of ''unrelaxed'' supercell calculations in which the Al atomic positions are constrained to that of ideal pure Al. The difference between the unrelaxed and relaxed calculations gives the energy gained by relaxation of Al atoms upon the insertion of a H atom. The energy gain upon relaxation for H in an O_h interstice is minimal (-0.04 eV), but a large relaxation accompanies H in T_d sites (-0.29 eV). The distinction between atomic relaxation for the two sites is so large that the site preference is reversed when the artificial unrelaxed geometry is considered (i.e., O_h sites are preferred). Thus, from this comparison, we conclude that atomic relaxations are a dominant physical effect controlling the site preference of H in Al. These results also could explain some of the early calculations that both reported O_h site preferences and did not allow for atomic relaxation.

B. Vibrational states of H in Al

We next consider vibrational states of H in Al, and their impact on site preference.

Zero-point vibrations. Harmonic vibrational frequencies of H in T_d and O_h sites in Al were calculated using the frozen-phonon dynamical matrix approach. The calculated zero-point frequencies and energetics are given in Table VI. Hydrogen in the smaller T_d site has higher vibrational frequencies than in the larger O_h site. Thus, the O_h site has a significantly lower zero-point energy than T_d. Although the difference between the zero-point energies in the T_d and O_h sites is large, it is not sufficient to reverse the T_d site preference found in the static, nonvibrating calculations above. *When both atomic relaxation and zero-point vibrations are included, H in Al is slightly energetically preferred in the T_d site (at $T=0$ K), in agreement with the low-temperature experimental results of Bugeat et al.*[12] The physical contributions to site preference of H in Al are summarized in Fig. 6. The above results do not consider the presence of defects in the Al matrix to which the hydrogen might bind. We describe below calculations that demonstrate the T_d site preference of H, even when strongly interacting with Al vacancies.

In Table VI we report the vibrational frequencies determined both harmonically and anharmonically, and using our frozen phonon approach compared with the Einstein model. First, we note that the frequencies calculated using the Einstein model are in good agreement with those obtained from the full frozen phonon dynamical matrix. While not surprising for the T_d site, where the H vibration is roughly 500 cm^{-1} above the highest Al frequency, this is noteworthy for the O_h site for which the calculated H frequency lies right near the top of the Al spectrum, forming a sharp peak in the phonon density of states centered at $\nu_{O_h}=354$ cm^{-1}. Inspection of vibrational eigenvectors $\mathbf{e}_j(i)$, where j is phonon mode and i is atom index, reveals that this peak has only 70% H character according to weights calculated as $\mathbf{e}_j^2(i)$. The remaining 30% are distributed over all Al atoms, which show a displacement pattern of the longitudinal acoustic (LA) X-point [100] zone-boundary mode. Furthermore, some hydrogen character is observed in the vibrations of the surrounding Al neighbors at frequencies near 250 cm^{-1}, which also correspond to the LA-phonon modes of Al. Since the intermixing between H and zone-boundary Al vibrations is not negligible, it is somewhat surprising that the agreement between a simple Einstein model and the full dynamical matrix calculation is so good.

The unusually low value of ν_{O_h} is a consequence of weak interactions between the host lattice and H in the O_h site. It is consistent with our finding of only a small amount of lattice relaxation around this impurity. However, it also suggests that anharmonic effects may be important. Indeed, the root-mean-square displacements of H atoms at $T=0$ are on the order of 0.2 Å, i.e., approximately 10% of the Al-H distance and considerably larger than the maximum displacement (0.04 Å) used in obtaining the harmonic dynamical matrix. For such large changes in the Al-H bond length anharmonic hard-core repulsion becomes important. To quantify the magnitude of anharmonic effects, we have calculated energy curves as functions of H displacements while keeping all Al atoms fixed at their equilibrium positions. These curves were obtained for displacements out to 0.4 Å along three principle symmetry directions: [100], [111], and [110]. The three-dimensional Schrödinger equation was then

TABLE V. Comparison of first-principles and experimentally observed energetics of H in Al. All energies are in eV: $\delta E(T_d - O_h)$ is the energy difference between hydrogen in tetrahedral and octahedral interstices. [$\delta E(T_d - O_h) < 0$ indicates that tetrahedral sites are favored.] ΔE_{trans} is the energy difference between hydrogen in the tetrahedral site and hydrogen in the transition state between tetrahedral and octahedral sites. ΔE_{imp} is the $T=0$ energy of the a hydrogen impurity in Al, relative to bulk Al and a H_2 molecule. Calculated results are for 32-atom cells, $16\times16\times16$ **k** points, and 237 eV cutoff. Calculations including zero-point effects indicated by an asterisk (*) are for a ''reduced mass'' model with a potential of the form of Eq. (1); otherwise, zero-point calculations employ a frozen phonon approach using supercells with 32 Al sites, as described in the text.

	Site preference	$\Delta E_{\text{imp}}(T_d)$	$\Delta E_{\text{imp}}(O_h)$	$\delta E(T_d - O_h)$	ΔE_{trans}
Expt.	T_d [a]	+0.67 [b]			+0.52±0.07 [g]
		+0.60 [c]			+0.17±0.02 [h]
		+0.65 [d]			+0.57 [i]
		+0.71 [d]			
		+0.65 [e]			
		+0.66 [f]			
GGA (relaxed+ZP-anharm*)	T_d	+0.71	+0.76	−0.05	
GGA (relaxed+ZP-harm)	T_d	+0.71	+0.75	−0.04	+0.15
GGA (relaxed)	T_d	+0.69	+0.82	−0.13	+0.18
GGA (unrelaxed)	O_h	+0.98	+0.86	+0.12	+0.19
LDA (relaxed)	T_d	+0.47	+0.52	−0.05	+0.16

[a]Reference 12.
[b]Reference 21.
[c]Reference 22.
[d]Reference 23.
[e]Reference 25.
[f]Reference 24.
[g]Reference 30.
[h]Reference 27.
[i]Reference 26.

solved in the basis of harmonic oscillator eigenstates. For H in the O_h site, where some intermixing of H and Al vibrations was found in the harmonic case, this Einstein-like model is justified *a posteriori* by our findings that anharmonic corrections increase the H frequency to approximately 100 cm^{-1} above the highest Al phonons; this effect should lead to a dramatic decrease in the intermixing of Al and H modes in comparison with the harmonic case. The resulting energy levels are sketched in Fig. 7, which also shows the energy curve along the [111] direction, through the T_d and O_h sites.

We find that anharmonic effects increase the ground-state energy in the O_h site by 30 meV, while the T_d site energy is almost unchanged (see Table VI). It is interesting that the calculated ground-state energy in the O_h site lies above the saddle-point energy of the transition state between the O_h

TABLE VI. First-principles calculated vibrations for H in Al. Unless otherwise indicated, all calculations are for supercells with 32 Al sites, using the frozen phonon approach as described in the text. Calculations using the Einstein model and a potential of the form of Eq. (1) are indicated by an asterisk (*). For comparison, calculated and experimental frequencies of the H_2 molecule are also shown.

Configuration	Harmonic		Anharmonic	
	ν (cm^{-1})	$E_{\text{zero-point}}$ (eV/H atom)	ν (cm^{-1})	$E_{\text{zero-point}}$ (eV/H atom)
H in Al				
H (T_d)	851, 851, 851	0.158		
H (T_d)*	819, 819, 819	0.153	831, 831, 831	0.155
H (O_h)	354, 354, 354	0.066		
H (O_h)*	277, 277, 277	0.051	435, 435, 435	0.081
H (T_d)+□	754, 888, 888	0.157		
H migration	1046, 1046, (284*i*)	0.130		
H_2 molecule				
H_2	4390	0.136		
H_2 (expt.)	4401	0.136		

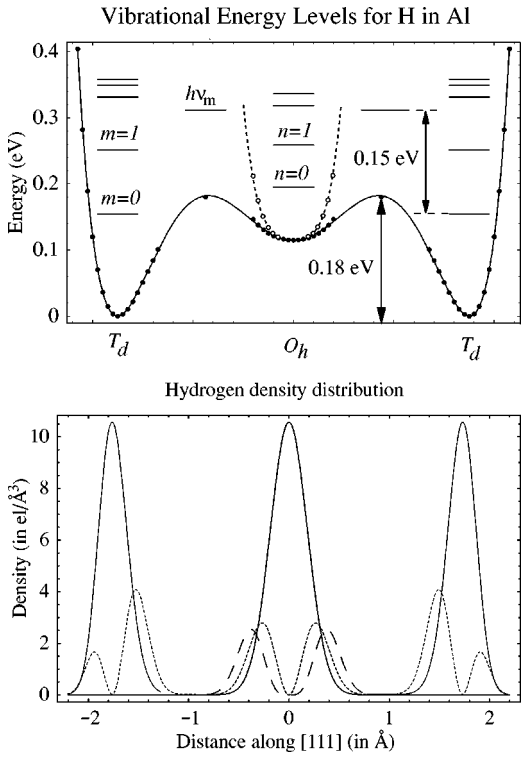

FIG. 7. Top panel: Potential energy for H displacements along the [111] diagonal through T_d and O_h sites. Anharmonic energy levels are shown as horizontal lines. Points are directly calculated values, while the solid line is a 12th-order polynomial fit. Dashed line shows the energy for H displacements along [100]. $h\nu_M$ is the zero-point energy at the saddle point for phonon displacements perpendicular to [111]. Bottom panel: Hydrogen density distributions in the lowest energy states on T_d and O_h sites. Solid lines give $n=0$ states, dotted lines give $n=1$ states, and dashed line gives the O_h state with $n=2$.

and T_d sites. One may even wonder if any bound states exist for H in the O_h site? Indeed, the true crystal states of H are delocalized. Localized Wannier-like states may be obtained from the crystal orbitals, and should have lifetimes that exceed the the characteristic vibrational periods by many orders of magnitude. Can such states be constructed for H on both O_h and T_d sites? We argue that they exist as the ground-state energy is higher than the confining potential only in a very small region around the saddle point. The width of this region is inversely proportional to the curvature of the potential surface in the direction perpendicular to [111]. This curvature is, of course, proportional to the vibrational frequencies ν_M of H in the saddle point (Table VI). To ''squeeze'' a H wave packet through the saddle point one must pay the price of localization energy, which is approximately given by $h\nu_M$. This energy level is shown in Fig. 7. We see that the effective height of the barrier is raised considerably. In fact, only states with $n=2$ and higher are unstable in this simple picture. Further support for the metastability of the H atom in the O_h site comes from inspecting the calculated anharmonic wave functions in the bottom panel of Fig. 7. It is seen that there is essentially no overlap between the T_d and O_h states. Since the transition probability is proportional to the square of the Hamiltonian matrix element taken between the initial and the final states,[72] it suggests that both the T_d and O_h states are sufficiently long lived at low temperatures. A direct numerical solution of the one-dimensional Schrödinger equation for the potential of Fig. 7 also gives very little overlap between the O_h- and T_d-localized H states. Since in one dimension the ''perpendicular phase space'' is infinitely large (i.e., $\nu_m=0$), and thus the ''localization barrier'' $h\nu_m$ does not exist, the 1D wave functions should be less localized than those in three dimensions.

Vibrational entropy. As seen from Fig. 7, only one excited state lies below the saddle point energy plus $h\nu_M$. Therefore, only the lowest excited state is available for thermal excitations contributing to the vibrational entropy of each type of site. We obtain that at $T=300$ K the entropy of H in the O_h site is 0.4 k_B higher than the entropy of H in the T_d site. This results in a relatively small 10 meV lowering of the $\delta E(O_h-T_d)$ free-energy difference. At high temperatures the Boltzmann factors for the higher $n\geqslant 2$ excited states become appreciable; as discussed above, these states may be delocalized, invalidating the concept of an entropy associated with a given site.

C. Dilute heat of solution

The dilute heat of solution is one of the few examples in the Al-H system where the majority of experimental reports are reasonably consistent. Many authors[21–25] have extracted the dilute heat of solution from solubility studies and found values in the range $+0.6$ to $+0.7$ eV. Some of these reported values are given in Table V.

We have calculated the dilute heat using supercells of N (N = 32, 64, 108) Al atoms:

$$\Delta E_{\mathrm{imp}}(\mathrm{H})=E(\mathrm{Al}_N\mathrm{H}_1)-[NE(\mathrm{Al})+\tfrac{1}{2}E(\mathrm{H}_2)]. \qquad (4)$$

The calculated dilute heats of solution are given in Table V, and compared with experimental reports. Our result (GGA) for the dilute heat of a static H impurity in a T_d site is 0.69 eV, in good agreement with the experimental reports. Calculation of the vibrational contributions to Eq. (4) shows that their effect on the dilute heat is quite small, due to the fact that the zero-point energies of the T_d impurity and H_2 molecule (first and third terms in Eq. (4), respectively) are quite similar (see Table VI), differing by only ~ 0.02 eV/H atom. Thus, including vibrational energies raises the dilute heat to 0.71 eV, still in good agreement with experimental reports.[73]

The LDA (static) result, 0.47 eV, is somewhat lower than both GGA and experiment, but as noted above, if the energy of the H_2 molecule is adjusted to bring the hydride formation energy into agreement with GGA, the dilute heat number for LDA becomes 0.60 eV. Thus, again we see that much of the difference between the LDA and GGA calculations can be traced to the energy of the H_2 molecule in Eq. (4).

Note that the artificial AlH rocksalt and zincblende compounds in Fig. 1 both possess an fcc sublattice of Al atoms, one Al atom per unit cell, with H in O_h and T_d positions, respectively. Our first-principles calculations give formation

energies of 0.40 and 0.38 eV/atom, respectively, or 0.80 eV/H atom for H in O_h coordination and 0.76 eV/H atom for T_d. These numbers are quite close to the supercells results in Table V of 0.82 (O_h) and 0.69 (T_d), thus demonstrating that even a ''one-atom-supercell'' [i.e., $N=1$ in Eq. (4)] is reasonably converged. Therefore, one must conclude that the H atoms do not appreciably interact with other H atoms in the presence of Al.

We should also comment on the recent paper of Lu *et al.*,[15] who used the same method as the present work (VASP-LDA), but found a dilute heat of -0.22 eV, compared with our LDA result of $+0.47$ eV. We believe that the source of this ~ 0.7 eV discrepancy can be traced to the fact that Lu *et al.* use different energy cutoffs in the three terms of Eq. (4), $E_{\mathrm{cut}}=350$ eV for the H impurity and the H_2 molecule, but $E_{\mathrm{cut}}=130$ eV for the calculation of pure Al. We have found that this low cutoff for pure Al gives a total energy that differs from a 350 eV calculation by 0.022 eV/atom. While this error may seem small, it is multiplied in Eq. (4) by the number of atoms in the supercell (32 in the case of Lu *et al.*), thus leading to an error of 0.70 eV in the dilute heat, and explaining the discrepancy. However, this error in Ref. 15 only pertains to their results that compare energetics of H-containing with non-H-containing systems. Results (such as the H migration barrier) that only involve H-containing cells, agree well with our calculations.

D. Diffusion and H-vacancy binding in Al

Measuring the diffusion coefficient of hydrogen in solid aluminum is hampered by the limited solubility of hydrogen. Existing measurements vary by orders of magnitude. Due to the low solubility, diffusion measurements are often performed at high temperatures near the melting point of Al, where there are an appreciable number of vacancies. Thus, the influence of vacancies (denoted by $\square$) on the diffusion of hydrogen is significant, and the H-$\square$ binding energy as well as the migration energy are important quantities in a study of hydrogen diffusion in Al.

Many measurements of the activation energy for diffusion of H in Al have been made. Most of the energies fall in the range between 0.4 and 0.6 eV (e.g., see Refs. 26 and 1 and references therein). For example: Linderoth[30] examined measured diffusivity data, and extracted the migration energy of H in Al as 0.52 ± 0.07 eV. Using a real-time dynamic technique under ultrahigh vacuum conditions in large grain aluminum (to avoid complications of porosity, surface contamination, oxide thickness, and grain size), Outlaw *et al.*[74] found an activation energy 0.49 eV.

Although it may initially appear as though there is consensus on an activation for H diffusion near 0.5 eV, the situation is complicated by considerations of H-defect binding: Hashimoto and Kino[28] measured the diffusivity of H in Al at high temperature and found an activation of 0.61 eV, close to the activation energy of self-diffusion in Al. However, at lower temperature, these authors found a much larger diffusivity than that extrapolated from high temperatures. They concluded that because there are more vacancies in equilibrium at high temperature, their diffusivity results could be explained by a large H-$\square$ binding. However, to test these assertions, Ishikawa and McLellan[26] used an electrolytic method to measure diffusion near room temperature. These authors found good agreement between their measured activation energy and previous high-temperature measurements. In other words, they found no such discrepancy as in the results of Hashimoto and Kino. Therefore, since there are essentially no vacancies in Al at ambient temperature, these authors suggested no particular mechanism for H diffusion that is keyed to migration of vacancies.

However, in addition to the work of Hashimoto and Kino,[28] many other measurements have pointed to a significant H-$\square$ interaction: Linderoth[30] analyzed measured diffusivity data from the literature, and ''corrected'' for the influence of H-$\square$ binding. From this analysis, the extracted H-$\square$ binding energy is 0.43 ± 0.07 eV. Monitoring D distributions in Al by an ion-induced nuclear reaction, Myers[31] analyzed the results using diffusion theory and found H-$\square$ binding of $+0.52\pm0.10$ eV. Positron annihilation experiments have yielded[75,76] a binding energy of 0.53 ± 0.03 eV. By measuring length change and lattice parameters of H introduced into high purity Al, Birnbaum *et al.*[29] showed the hydrogen was trapped at vacancies and that the composition of H and vacancies were roughly comparable. From these measurements, they estimated a H-$\square$ binding of 0.48 eV.

Recently, this problem has been reexamined by Young and Scully.[27] By isothermal and constant heating rate desorption techniques, they measured diffusion and trapping of H in Al. Somewhat surprisingly, these authors found a very small activation energy compared with all previous results: 0.17 eV.[78] However, they observed two H trapping sites with binding energies 0.28 ± 0.18 and 0.71 ± 0.33 eV, which they assigned to dislocations and vacancies, respectively. These authors suggested that many previous diffusivities may actually be trap affected, thus providing a possible explanation of the widely varying values.

Several theoretical papers have also addressed the issue of H-$\square$ binding in Al: Popovic *et al.*[19,20] used a nonlinear response theory to obtain approximately self-consistent electron densities surrounding a proton and found that the substitutional site is considerably lower in energy (1.23 eV) than either an O_h or T_d interstitial sites. From a self-consistent LDA jellium calculation Larsen and Norskov[13] found the T_d site to be most stable with a heat of solution of $+1.3$ eV and found a H-$\square$ binding of approximately 1 eV. Effective medium theory calculations of this binding[31] have yielded a value of 0.52 eV, in good agreement with the experimental results.

From our (N atom) supercell calculations, we have calculated the H-$\square$ binding energy:

$$\delta E(\mathrm{H}-\square)=E(\mathrm{Al}_{N-1}\mathrm{H}_1\square_1)+N\times E(\mathrm{Al})-E(\mathrm{Al}_{N-1}\square_1)-E(\mathrm{Al}_N\mathrm{H}_1). \quad (5)$$

From Eq. (5), it is apparent that calculation of the vacancy formation energy in Al, ΔE_{vac}, is a necessary byproduct of the H-$\square$ binding calculation. ΔE_{vac} has been calculated previously from first-principles approaches by many authors.

TABLE VII. Comparison of first-principles and experimentally observed energetics of H-□ (denoted by □) interactions in Al. All energies are in eV: ΔE_{vac} is the vacancy formation energy in Al. $\Delta E_{\mathrm{imp}}(T_d+\square)$ and $\Delta E_{\mathrm{imp}}(O_h+\square)$ are the formation energies of H-□ pairs. $\Delta E_{\mathrm{imp}}(\mathrm{sub})$ is the formation energy for H in a substitutional site. $\delta E(\mathrm{H}-\square)$ is the H-□ binding energy between H in T_d sites and vacancies. Calculated results are for 32-atom cells, 16×16×16 or higher **k**-points, and 237 eV cutoff. Note that zero-point effects are not included in the calculated results in this table.

	ΔE_{vac}	$\Delta E_{\mathrm{imp}}(T_d+\square)$	$\Delta E_{\mathrm{imp}}(O_h+\square)\mathrm{NN}$	$\Delta E_{\mathrm{imp}}(O_h+\square)2\mathrm{NN}$	$\Delta E_{\mathrm{imp}}(\mathrm{sub})$	$\delta E(\mathrm{H}-\square)$
Expt.	+0.67 [a]					+0.43±0.07 [c]
						+0.53±0.03 [d]
						+0.52±0.10 [e]
GGA (relaxed)	+0.54 [b]	+0.90	+1.14	+1.40	+1.76	+0.33
GGA (unrelaxed)	+0.63	+1.06	+1.28	+1.54	+1.87	+0.55

[a]References 82 and 83.

[b]Carling *et al.* (Ref. 81) have recently shown that the discrepancy between the experimental and GGA-calculated vacancy formation energy in Al may be resolved via a ''surface'' correction to the electron correlation effects.

[c]Reference 30.

[d]Reference 75.

[e]Reference 31.

(See, e.g., Refs. 44, 45, 79–81 and references therein.) Our GGA result of $\Delta E_{\mathrm{vac}}=0.54$ eV agrees well with the result (0.54 eV) of Carling *et al.*[81], who have recently shown that the discrepancy between the GGA-calculated and experimental vacancy formation energy in Al (0.67 ± 0.03 eV[82]) may be resolved via a ''surface'' correction to the electron correlation effects. However, these authors also suggest that this correction cancels when considering *binding* between defects, such as the H-□ interaction considered here.

We have performed calculations for the H/□ in several different positions: (1) T_d H, nearest neighbor to □, (2) O_h H, nearest neighbor to □, (3) O_h H, next-nearest neighbor to □, and (4) substitutional H (H on the □ site). The calculated results are given in Table VII. We note several points: (a) Even in the presence of vacancies, the interstitial T_d position is still favored over O_h and substitutional positions. The equilibrium position of H in the H+□ pair is off-center, displaced from the nominal tetrahedral site by approximately 0.15 Å. (b) The first-principles results show a substantial H-□ binding (with T_d H) of 0.33 eV. This value is qualitatively consistent with the large binding energy inferred from a variety of diffusion data. However, the value is somewhat smaller than the estimates inferred from experiment. (c) Although smaller, there is a binding of vacancies with NN O_h H of 0.22 eV. For NNN O_h H-□ pairs, the defects do not interact strongly, with a binding near zero (−0.04 eV). (d) The substitutional site is quite high in energy (0.86 higher than the T_d H-□ pair). Thus, even for a NN H-□ pair, the H atom will not ''fall into'' the vacant site. This result is in qualitative contrast with the early jellium results of Popovic.[19] (e) Vibrational calculations of H in the T_d sites show that one of the three H vibrations is slightly softened in the presence of vacancies, while the other two are stiffened somewhat (Table VI). These effects nearly balance, giving very similar zero-point energies of H in the presence (0.157 eV) and absence (0.158 eV) vacancies. Thus, the effect of zero-point energy on the H-□ binding is very small.

We have also performed calculations of the migration energy for diffusion both with and without an Al vacancy. A schematic figure of the migration paths and barriers is also given in Fig. 8.

Diffusion of H with no vacancies. When there are no vacancies present, there is a small energy barrier (0.18 eV) separating the T_d and O_h positions. This small migration energy is in excellent agreement with the recent results of Young and Scully[27] and also is consistent with the recent first-principles calculations of Lu *et al.*[15]

Diffusion of H in the presence of vacancies. For H in a T_d position with a nearest-neighbor Al vacancy, there are two possible pathways for the H atom to diffuse from its position to a neighboring O_h site. One of these paths leads to an O_h site that is a nearest neighbor to the vacancy, and the other leads to an O_h site that is second-nearest neighbor to the □. We call these ''Path 1'' and ''Path 2,'' respectively, and they are shown in Fig. 8(a). ''Path 2'' takes the H atom on a direct pathway away from the vacancy. For each of these two paths, we also consider the subsequent migration from the O_h site to a T_d site, second-nearest neighbor to the □.

Although in the absence of vacancies, the migration energy was relatively low (0.18 eV without zero-point corrections), in the presence of vacancies, moving the H from the T_d site to the O_h position involves breaking the H-□ binding energy (0.33 eV), and so the calculated barrier, 0.54 eV, is roughly equal to the migration energy without vacancies (0.18 eV) plus the H-□ binding (0.33 eV). Figure 8(b) shows the calculated energetics for both paths considered. The first step in ''Path 1'' (to the $O_h+\square$ NN position) has an energy barrier of only 0.28 eV, because there is still significant binding (0.22 eV, see Table VII) between the H and □ in this position. In this case, the second step (to the $T_d+\square$ 2NN position) that involves breaking the $O_h+\square$ NN binding energy, resulting in a barrier of 0.30 eV. However, the overall barrier for this migration path is shown in Fig. 8 and is 0.54 eV. For ''Path 2,'' the first step involves migration to a site ($O_h+\square$ 2NN) with no significant binding, and thus the migration energy is large, with the $O_h+\square$ 2NN site even becoming an unstable saddle point on the energy surface. In the second step in ''Path 2,'' the binding with the vacancy is

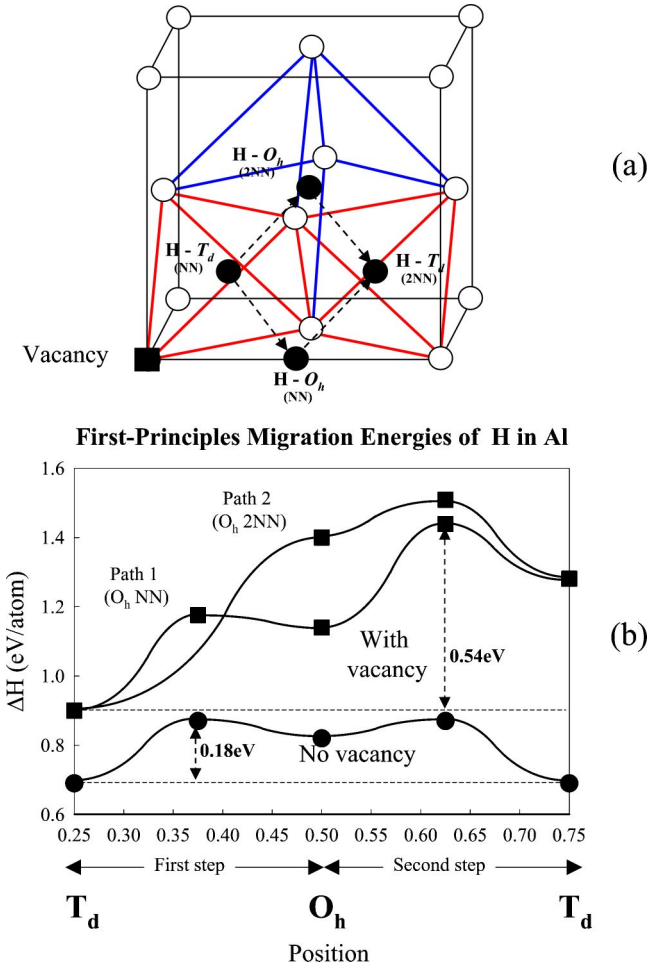

FIG. 8. First-principles calculated migration energies of H in Al. (a) The considered pathway connecting a tetrahedral position $(\frac{1}{4}\ \frac{1}{4}\ \frac{1}{4})$ in units of the lattice parameter of Al to an octahedral position $(\frac{1}{2}\ \frac{1}{2}\ \frac{1}{2})$. (b) Energetics along the pathway in the absence and presence of vacancies. When there are no vacancies present, there is a small energy barrier (0.18 eV) separating the T_d and O_h positions. However, when a vacancy is present at (000), moving the H from the T_d site to the O_h position involves breaking the H-□ binding energy (0.33 eV), thus resulting in a much larger barrier to diffusion. Calculated points are shown, and curves are drawn schematically merely as a guide to the eye. Note that zero-point effects are not included in the energetics of this figure.

essentially broken already, and so this energetic pathway looks very similar to that of the case with no vacancies. Thus, these calculations are consistent with the assertion of Young and Scully,[27] and the strong H-□ binding can reconcile their diffusion results (with a small activation energy) with previous results finding a larger activation of ~0.5 eV.

The reader should note that our discussion of diffusion has implicitly been couched within the framework of classical transition-state theory. However, as we have seen, H does not always behave classically, and much work has gone into developing a quantum theory of diffusion.[72,84,85] At low temperatures, quantum tunneling occurs whereas classical ''hopping'' occurs at high temperatures. There are intermediate crossover and quantum correction regimes as well. A full connection between our results and the quantum theory of diffusion is beyond the scope of this work; however, we suggest that future work in this area could be fruitful.

Finally, in a series of papers, McLellan *et al.* (see e.g., Refs. 86,87 and references therein) have modeled hydrogen diffusion, accounting for the substantial H-□ interaction. However, to get numerical values out of these diffusion models, parameters such as the H-□ binding energy, site preference, etc., must be input. Since some of the quantities used in previous models (particularly those from early jellium-type calculations) have been somewhat suspect, it would be interesting to repeat these types of analyses using as input our first-principles derived quantities.

V. SUMMARY

Using a combination of density functional total energy, linear response, and frozen phonon calculations, we have performed a systematic investigation of the energetics and stability of the Al-H system.

Aluminum hydride. By comparing energetics and structural properties, we have determined that the majority of the difference between LDA and GGA descriptions lies not in the solid-state compounds, but rather in the description of the H_2 molecule. As GGA provides a more accurate picture of H_2, it also provide quantitatively more accurate energetics of the AlH_3 hydride as well as a more accurate heat of solution for H in Al. The GGA predicted structural properties of AlH_3 also agree well with experiment. Linear response calculations (within the LDA) of AlH_3 yield important insights into the vibrational and thermodynamic properties of this compound. By combining the static $T=0$ formation energy of AlH_3, calculated zero-point energies, as well as experimental equation of state data for H_2, we have demonstrated that, consistent with experimental calorimetry data, the metastable AlH_3 compound has a weak, negative formation enthalpy at ambient conditions, but a more strongly positive formation free energy.

Metal hydrides. To ascertain more about the applicability of density functional calculations to the energetics of metal hydride systems, we have performed a series of calculations for *M*-H hydrides: *M* = Al, Ba, Ca, K, Mg, La, Li, Na, Ni, Pd, Sc, Sr, Ti, V, and Y. The formation energies of these hydrides spans a range between ~0 and −100 kJ/0.5 mol H_2, and the agreement between calculated $T=0$ static energies and measured enthalpies is within 10–15 kJ/0.5 mol H_2. Inclusion of zero-point energies and other dynamic contributions in the calculations would likely increase the agreement with experiment. The GGA calculations are therefore shown to provide a good predictor for a formation energies for a wide range of metal hydrides.

Site preference of H in Al. For Al-H, we find that both atomic relaxation and anharmonic vibrational effects play an important role in the tetrahedral versus octahedral interstitial site preference of H in Al. In static, unrelaxed calculations, H energetically prefers the larger O_h site. However, atomic relaxation is larger in the T_d site, and the energetic effect of these relaxations overwhelms the static site preference, yielding a T_d favored site. However, vibrational frequencies of H

in the T_d site are larger than in the O_h site, thus giving a larger zero-point energy in the T_d site. When all contributions are considered, the calculations predict a small preference for H in T_d sites and $T=0$, consistent with the one experimental report of site preference. We have also shown that the calculated heat of solution of H in Al is large and positive (+0.71 eV), consistent with experimental solubility data and with Al as an endothermic hydrogen absorber.

Diffusion and defect binding of H in Al. In an ideal bulk Al, a calculation of the migration energy of H between the T_d and O_h sites give 0.18 eV. However, based on previous reports, we have also investigated the interaction between H and Al vacancies, finding a large binding energy of 0.33 eV. For calculations of H migrating away from an Al vacancy, the migration energy increases to 0.54 eV. Therefore, consistent with the recent study of Young and Scully,[27] we find that vacancy trapping of H can provide at least part of the explanation for the disparity between observed H migration barriers reported in the literature.

ACKNOWLEDGMENTS

We would like to acknowledge many helpful discussions about various aspects of metal-hydrogen systems with the following: John Allison, Alex Bogicevic, Gerd Ceder, Ali Chirazi, Steve Harris, Ken Hass, Jeff Hoyt, Bill Schneider, Ellen Stechel, and Jake Zindel. Research at Northwestern was sponsored by the U.S. Department of Energy, Office of Basic Energy Sciences, Materials Science Division, under Contract No. DE-FG02-01ER45910. Work at UCLA was funded by the U.S. Department of Energy, Office of Power Technologies, Hydrogen Program Office under Contract No. DE-AC36-83CH10093.

[1] *Hydrogen in Metals III*, edited by H. Wipf (Springer, New York, 1997).
[2] *Hydrogen in Intermetallic Compounds I*, edited by L. Schlapbach (Springer, New York, 1988).
[3] *Hydrogen in Metals*, edited by G. Alefeld (Springer, New York, 1978).
[4] H. Wenzl, Int. Metall. Rev. **27**, 140 (1982).
[5] *Phase Diagrams of Binary Hydrogen Alloys*, edited by F. D. Manchester (ASM, Materials Park, OH, 2000).
[6] *Metal Hydrides*, edited by W. M. Mueller, J. P. Blackledge, and G. G. Libowitz (Academic Press, New York, 1968).
[7] J. E. Hatch, *Aluminum: Properties and Physical Metallurgy* (ASM, Ohio, 1998).
[8] L. F. Mondolfo, *Aluminum Alloys–Structure and Properties* (Butterworth, London, 1976).
[9] P.D. Lee, A. Chirazi, and D. See, J. Light Metals **1**, 15 (2001).
[10] P.D. Lee and J.D. Hunt, Acta Mater. **49**, 1383 (2001).
[11] F. D. Manchester and A. San-Martin, in *Phase Diagrams of Binary Hydrogen Alloys*, edited by F. D. Manchester (ASM, Materials Park, OH, 2000), p. 4.
[12] J.P. Bugeat, A.C. Chami, and E. Ligeon, Phys. Lett. **58A**, 127 (1976).
[13] D.S. Larsen and J.K. Norskov, J. Phys. F: Met. Phys. **9**, 1975 (1979).
[14] G. Solt, M. Manninen, and H. Beck, J. Phys. F: Met. Phys. **13**, 1379 (1983).
[15] G. Lu, D. Orlikowski, I. Park, O. Politano, and E. Kaxiras, Phys. Rev. B **65**, 064102 (2002).
[16] M. Ruda, D. Farkas, and J. Abriata, Phys. Rev. B **54**, 9765 (1996).
[17] M. Manninen and R.M. Nieminen, J. Phys. F: Met. Phys. **9**, 1333 (1979).
[18] F. Perrot and M. Rasolt, Phys. Rev. B **23**, 6534 (1981).
[19] Z.D. Popovic and M.J. Scott, Phys. Rev. Lett. **33**, 1164 (1974).
[20] Z.D. Popovic, M.J. Scott, J.P. Carbotte, and G.R. Piercy, Phys. Rev. B **13**, 590 (1976).
[21] R.A.H. Edwards and W. Eichenauer, Scr. Metall. **14**, 971 (1980).
[22] W. Eichenauer, K. Hattenbach, and A. Pebler, Z. Metallkd. **52**, 682 (1961).
[23] W. Eichenauer, Z. Metallkd. **59**, 613 (1968).
[24] M. Ichimura, H. Katsuta, Y. Sasajima, and M. Imabayashi, J. Phys. Chem. Solids **49**, 1259 (1988).
[25] H. Sugimoto and Y. Fukai, Acta Metall. Mater. **40**, 2327 (1992).
[26] T. Ishikawa and R.B. McLellan, Acta Metall. **34**, 1091 (1986).
[27] G.A. Young, Jr. and J.R. Scully, Acta Mater. **46**, 6337 (1998).
[28] E. Hashimoto and T. Kino, J. Phys. F: Met. Phys. **13**, 1157 (1983).
[29] H.K. Birnbaum, C. Buckley, F. Zeides, E. Sirois, P. Rozenak, S. Spooner, and J.S. Lin, J. Alloys Compd. **253-254**, 260 (1997).
[30] S. Linderoth, Philos. Mag. Lett. **57**, 229 (1988).
[31] S.M. Myers, F. Besenbacher, and J.K. Norskov, J. Appl. Phys. **58**, 1841 (1985).
[32] P. Hohenberg and W. Kohn, Phys. Rev. **136**, B864 (1964).
[33] W. Kohn and L.J. Sham, Phys. Rev. **140**, A1133 (1965).
[34] D. Vanderbilt, Phys. Rev. B **41**, 7892 (1990).
[35] G. Kresse and J. Hafner, J. Phys.: Condens. Matter **6**, 8245 (1994).
[36] G. Kresse and J. Hafner, Phys. Rev. B **47**, 558 (1993).
[37] G. Kresse, Ph.D. thesis, Technische Universität Wien, 1993.
[38] G. Kresse and J. Furthmüller, Comput. Mater. Sci. **6**, 15 (1996).
[39] G. Kresse and J. Furthmüller, Phys. Rev. B **54**, 11 169 (1996).
[40] D.M. Ceperley and B.J. Alder, Phys. Rev. Lett. **45**, 566 (1980).
[41] J.P. Perdew and A. Zunger, Phys. Rev. B **23**, 5048 (1981).
[42] J. P. Perdew, in *Electronic Structure of Solids 1991*, edited by P. Ziesche and H. Eschrig (Akademie Verlag, Berlin, 1991), Vol. 11.
[43] H.J. Monkhorst and J.D. Pack, Phys. Rev. B **13**, 5188 (1976).
[44] N. Chetty, M. Weinert, T.S. Rahman, and J.W. Davenport, Phys. Rev. B **52**, 6313 (1995).
[45] D.E. Turner, Z.Z. Zhu, C.T. Chan, and K.M. Ho, Phys. Rev. B **55**, 13 842 (1997).
[46] Y. Chen, C.L. Fu, K.-M. Ho, and B.N. Harmon, Phys. Rev. B **31**, 6775 (1985).
[47] G. K. Horton and A. Maradudin, *Dynamical Properties of Solids* (North-Holland, New York, 1974).
[48] V. Ozoliņš and M.D. Asta, Phys. Rev. Lett. **86**, 448 (2001).
[49] J.W. Turley and H.W. Rinn, Inorg. Chem. **8**, 18 (1969).

[50] In the comparison between calculated and experimental lattice parameters, zero-point effects are not considered, although they could influence such a comparison.
[51] H. Smithson, D. Morgan, A.V. der Ven, C. Marianetti, A. Predith, and G. Ceder, Phys. Rev. B **66**, 144107 (2002).
[52] K. Miwa and A. Fukumoto, Phys. Rev. B **65**, 155114 (2002).
[53] G.C. Sinke, L.C. Walker, F.L. Oetting, and D.R. Stull, J. Chem. Phys. **47**, 2759 (1967).
[54] A.I. Kolesnikov, M. Adams, V.E. Antonov, N.A. Chirin, E.A. Goremychkin, G.G. Inikhova, Y.E. Markushkin, M. Prager, and I.L. Sashin, J. Phys.: Condens. Matter **8**, 2529 (1996).
[55] It should be remembered that the vibrational properties of AlH_3 are calculated using the LDA and the *experimental* lattice parameters. By performing separate linear-response calculation at the *LDA equilibrium* lattice geometry we find that the zero-point energy increases by only 6 meV/atom. Differences in the calculated phonon frequencies between the LDA and GGA are usually attributed to increase in the calculated equilibrium lattice constant. Since the GGA lattice constants of AlH_3 are already close to the experimental values, this too is expected to be a small effect.
[56] We note that the enthalpy of AlH_3 increases by much less (only 16 meV/atom) than $3k_BT$ because its Debye temperature is very high. For instance, at $T=300$ K its heat capacity C_V is only $1.26k_B$ (see Fig. 3). For Al, $C_V=2.8k_B$, and the corresponding increase in H_{vib} is 45 meV/atom, i.e., about half of the $3k_BT$ value implied by the classical Dulong-Petit law.
[57] The value of the enthalpy of H_2, $H=\frac{7}{2}k_BT$, is idealized, but is within a few percent of the experimentally determined equation of state information for H_2: $H=8506$ J at 300 K and $P=1$ bar, or $H\sim 3.4k_BT$ [see H. Hemmes, A. Driessen, and R. Griessen, J. Phys. C **19**, 3571 (1986)].
[58] P. W. Atkins, *Physical Chemistry* (Freeman, New York, 1986).
[59] C. Wolverton and K.C. Hass, Phys. Rev. B **63**, 024102 (2000).
[60] C. Wolverton, Acta Mater. **49**, 3129 (2001).
[61] L.A. Curtiss, K. Raghavachari, P.C. Redfern, and J.A. Pople, J. Chem. Phys. **106**, 1063 (1997).
[62] *CRC Handbook of Chemistry and Physics*, 83rd ed., edited by D. R. Lide (CRC Press, New York, 2002).
[63] B. Bogdanovic, R.A. Brand, A. Marjanovic, M. Schwickardi, and J. Tölle, J. Alloys Compd. **302**, 36 (2000).
[64] J.-L. Martins, Phys. Rev. B **41**, 7883 (1990).
[65] H.-J. Tao, K.-M. Ho, and X.-Y. Zhu, Phys. Rev. B **34**, 8394 (1986).
[66] G.N. Garcia, J.P. Abriata, and J.O. Sofo, Phys. Rev. B **59**, 11 746 (1999).
[67] L.G. Hector, J.F. Herbst, and T.W. Capehart, J. Alloys Compd. **353**, 74 (2003).
[68] M. E. A. y de Dompablo and G. Ceder, J. Alloys Compd. **364**, 6 (2004).
[69] M.J. Puska and R.M. Nieminen, Phys. Rev. B **29**, 5382 (1984).
[70] G. Lu, Q. Zhang, N. Kioussis, and E. Kaxiras, Phys. Rev. Lett. **87**, 095501 (2001).
[71] A.V. Irodova *et al.*, Sov. Phys. Crystallogr. **33**, 453 (1988).
[72] C.P. Flynn and A.M. Stoneham, Phys. Rev. B **1**, 3966 (1970).
[73] We note that we have not included the $7/2k_BT$ contribution to the enthalpy of H_2 in comparing with the experimental dilute heat of solution. Experimental estimates of the dilute heat are extracted from solubility measurements. Because the $7/2k_BT$ is an *enthalpic* contribution that is linear in T, in fitting solubility data to a function of the form $\exp(S/k)\exp(-H/kT)$, this term, unless explicitly included in the analysis could appear as though it were an "entropic" term in the fit.
[74] R.A. Outlaw, D.T. Peterson, and F.A. Schmidt, Scr. Metall. **16**, 287 (1982).
[75] S. Linderoth, H. Rajainmaki, and R.M. Nieminen, Phys. Rev. B **35**, 5524 (1987).
[76] H. Rajainmaki, S. Linderoth, R.M. Nieminen, and H.E. Hausen, Mater. Sci. Forum **16**, 611 (1987).
[77] W. Eichenauer and J. Markopoulos, Z. Metallkd. **65**, 649 (1974).
[78] It is also perhaps worth noting that Eichenauer (Ref. 77) has measured H diffusion in *liquid* Al and found an activation energy of 0.2 eV, similar in magnitude to the small value observed by Young and Scully (Ref. 27) and also calculated here in *solid* Al.
[79] A.D. Vita and M.J. Gillan, J. Phys.: Condens. Matter **3**, 6225 (1991).
[80] T. Hoshino, N. Papanikolaou, R. Zeller, P.H. Dederichs, M. Asato, T. Asada, and N. Stefanou, Comput. Mater. Sci. **14**, 56 (1999).
[81] K. Carling, G. Wahnström, T.R. Mattsson, A.E. Mattsson, N. Sandberg, and G. Grimvall, Phys. Rev. Lett. **85**, 3862 (2000).
[82] P. Ehrhart, P. Jung, H. Schulta, and H. Ullmaier, in *Atomic Defects in Metals*, edited by H. Ullmaier, Landolt-Börnstein, New Series, Group III, Vol. 25 (Springer-Verlag, Berlin, 1990).
[83] T. Hehenkamp, J. Phys. Chem. Solids **55**, 907 (1994).
[84] P. Hänggi, P. Talkner, and M. Borkovec, Rev. Mod. Phys. **62**, 251 (1990).
[85] H. Grabert and H.R. Schober, Top. Appl. Phys. **73**, 5 (1997).
[86] R.B. McLellan, Scr. Metall. **17**, 1237 (1983).
[87] J. Mao and R.B. McLellan, J. Phys. Chem. Solids **62**, 1285 (2001).